# Effect of γ-ray irradiation on breakdown voltage, ideality factor, dark current and series resistance of GaAs p–i–n diode

Vinu R.V. Pillai [a,1], Shailesh K. Khamari [a], V.K. Dixit [a,*], T. Ganguli [b], S. Kher [a], S.M. Oak [a]

[a] Semiconductor Laser Section, Solid State Laser Division, Raja Ramanna Centre for Advanced Technology, Indore 452013, M. P., India
[b] Indus Synchrotrons Utilisation Division, Raja Ramanna Centre for Advanced Technology, Indore 452013, M. P., India

## ABSTRACT

Effect of $^{60}$Co γ-ray radiation with $1 \times 10^{16}$ γ/cm$^2$ fluence on the ideality factor, saturation current and series resistance for two separate junctions $p$–$i$ and $i$–$n$ of $p$–$i$–$n$ diode are studied by using temperature dependent current–voltage measurements and β model analysis. After γ-ray irradiation, the resistance of $p$–$i$–$n$ diode increases from 858 to 2789 Ω. This is due to the fact that unintentional impurities (mainly carbon) present in the $i$-region change their positions from Gallium to Arsenic sites and subsequently transform them to the acceptor like states. The dark and saturation current decrease following the γ-ray irradiation because of the reduced electron mobility and the compensation of majority carriers by the acceptor like trap states. In addition, the ideality factor of $p$–$i$ junction decreases from 1.5 to 1.2 while for the $i$–$n$ junction it increases from 7.2 to 8 after irradiation at 300 K. The ideality factor for the second junction is enhanced due to the increased recombination probability of carriers at the trap centers in the intrinsic region. Positive temperature coefficient of the breakdown voltage confirms that the avalanche multiplication process is responsible for the junction breakdown. Further, the breakdown voltage increases after the irradiation because of the scattering of charge carriers from the radiation induced defects.

© 2012 Elsevier B.V. All rights reserved.

## Introduction

Out of all the electronic components, semiconductor devices are the most sensitive to the radiation induced damages caused by energetic γ-rays, electrons, neutrons and ions. An exposure of these devices to such radiations results in the creation of considerable amount of lattice defects [1–4]. However, the nature of defects formed depends on the type of energetic radiation. While irradiation with the γ-rays and electrons produces mainly isolated point defects, irradiation with heavier ions produces more complex cluster of defects [4–7]. These defects affect the properties of materials in a number of ways including decrease of the carrier concentration in the base material, reduction of the minority carrier lifetime, decrease in the mobility of carriers and the radiation induced order–disorder transitions [8–12]. It affects the characteristic and performance of metal–semiconductor Schottky diodes, metal–oxide–semiconductor devices, $p$–$i$–$n$ detectors and solar cells etc. Considering the sensitivity of semiconductor devices to the impinging radiation and the large number of junctions required in today's circuitry, a lot of attention is being given to determine the

effects of radiation on the electrical characteristics of GaAs semiconductor devices [13–20]. To study the effect of point defects on the performance of devices, $^{60}$Co γ-ray is the most convenient source. In view of this, in our recent work, we have highlighted the effect of $^{60}$Co γ-ray irradiation on the properties of GaAs $p$–$i$–$n$ diode [21]. From the measurement of charge carrier mobility, leakage current and photoluminescence, we identified some of the defects which were responsible for the observed behavior. Here, we present the effect of $^{60}$Co γ-ray radiation on the reverse breakdown voltage ($V_B$), ideality factor ($\eta$), dark current ($I_d$), saturation current ($I_o$) and the series resistance ($R_s$) of GaAs $p$–$i$–$n$ diode at relatively higher dose (105 kGy). Further, in the ideality factor calculation by Shockley–Read–Hall theory, one assumes that the carrier recombination takes place via point defects [22]. Therefore, the effect of gamma irradiation on $\eta$ needs to be properly evaluated. Generally, the ideality factor of a $p$–$i$–$n$ diode is determined from an exponential diode equation using current–voltage ($I$–$V$) curve. However, for the correct description of the two linear regions in the log ($I$) vs. $V$ graph of a $p$–$i$–$n$ device, this single exponential equation is not sufficient. To address this issue, an elaborate model has been proposed recently, which takes into account the two junctions separately by using a curvature function analysis [23,24]. We understand that the junction properties like ideality factor, saturation current and series resistance could be estimated more accurately by using the recent model. We therefore

estimate junction properties by evaluating different parameters ($R_s$, $\eta$, $V_B$, $I_o$) using the curvature function ($\beta$) analysis for pristine and $\gamma$-ray irradiated $p$–$i$–$n$ diodes in the temperature range of 125–300 K. Furthermore, from the temperature dependent breakdown voltage, we identify the mechanism responsible for the junction breakdown.

## Growth, fabrication of $p$–$i$–$n$ diode and measurement procedures

GaAs epilayers of $p$–$i$–$n$ diode structures were grown on semi-insulating GaAs substrate at 700 °C using MOVPE. Trimethyl Gallium (TMGa) and Arsine (AsH$_3$) were used as the precursors. The intrinsic ($i$) layer of GaAs (4 µm thick) showed predominantly n-type behavior with an electron mobility of 78262 cm$^2$/Vs at 77 K. Donor and acceptor densities ($N_D$ and $N_A$) were $1.09 \times 10^{15}$ cm$^{-3}$ and $4.4 \times 10^{14}$ cm$^{-3}$, respectively [25]. The background dopant concentration was because of the unintentional impurities coming from the precursors used in the MOVPE growth process which predominantly occupy the Gallium sites [21]. These impurities were mainly carbon, incorporated from the Trimethyl Gallium precursor. The $i$ layer of 4 µm thickness was sandwiched between 300 nm of p-type (acceptor density $\sim 2 \times 10^{18}$ cm$^{-3}$) and 300 nm of n-type (donor density $\sim 10^{18}$ cm$^{-3}$) layers to form the $p$–$i$–$n$ diode structure. 2% Silane (SiH$_4$) in H$_2$ and Diethyl Zinc (DEZn) were used for $n$- and p-type doping, respectively. Ohmic contacts were made using the thermal evaporation of Ti/Pt/Au and Au-Ge/Ni/Au at $2-5 \times 10^{-6}$ mbar vacuum for $p$- and n-type, respectively and subsequent rapid thermal annealing of the samples at 450 °C for 50 s in nitrogen ambient. The MESA structures of GaAs $p$–$i$–$n$ diode were fabricated by wet chemical etching with H$_3$PO$_4$:CH$_3$OH:H$_2$O$_2$ (3:6:1) solution [26]. Irradiations experiments were carried out at room temperature in a 2490 Ci $^{60}$Co gamma chamber [27] and the electrical measurements were carried out immediately after irradiation. The fluence equivalents were calculated from the known activity of $\gamma$-ray source at the time of irradiation. Attenuation coefficient of $\gamma$-ray emitted from $^{60}$Co (1.17 MeV and 1.33 MeV) in GaAs is about 1 cm$^{-1}$ and the thickness of the active region in the irradiated device is only 4 µm. Therefore, it can be assumed safely that the entire device is irradiated uniformly. In our previous studies, we observed that the irradiation effects are substantial when the radiation dose is higher than 50 kGy ($5 \times 10^{15}$ $\gamma$/cm$^2$ fluence) [21]. Hence, here we present our studies for higher irradiated doses of 105 kGy ($1 \times 10^{16}$ $\gamma$/cm$^2$ fluence). Two sets of identical devices, each set containing nine devices, were processed simultaneously. Out of the two sets, one was irradiated with a radiation dose of 105 kGy ($1 \times 10^{16}$ $\gamma$/cm$^2$) whereas the other was used for the pristine measurement. There are statistical deviations from device to device and are highlighted in the figures by including appropriate error bars. Temperature dependent $I$–$V$ measurements for pristine and irradiated $p$–$i$–$n$ diodes were carried out in an indigenously developed close cycle refrigerator and using a current–voltage source measurement unit (Keithley 238) [28].

## Results and discussion

The $I$–$V$ characteristic of a real diode containing a series resistance is expressed by single exponential Shockley expression $V = 1/\alpha \ln (I/I_0 + 1) + IR_s$, where $\alpha = q/\eta kT$, $T$ is the measured diode temperature, $q$ is the electron charge, $\eta$ is the ideality factor and $k$ is the Boltzmann constant. However, when an equivalent circuit of GaAs $p$–$i$–$n$ diode is considered, it shows two junction diodes and a resistance connected in series. The schematic structure and corresponding equivalent circuit of a GaAs $p$–$i$–$n$ diode are shown
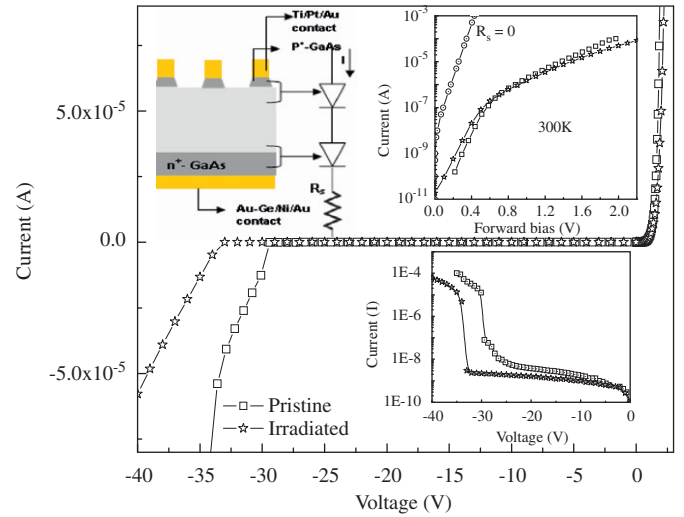


Fig. 1. Schematic structure of fabricated GaAs $p$–$i$–$n$ diode and its equivalent circuit consisting of two diodes connected in series along with a series resistance. Inset shows the forward and reverse bias $I$–$V$ characteristics of the pristine and irradiated diode.

in Fig. 1. Hence, the $I$–$V$ characteristic for this equivalent circuit of GaAs $p$–$i$–$n$ diode can be expressed as [29]

$$V \frac{1}{\alpha_1} \ln \left( \frac{I}{I_{o1}} + 1 \right) + \frac{1}{\alpha_2} \ln \left( \frac{I}{I_{o2}} + 1 \right) IR_s \tag{1}$$

where $\alpha_1 = q/\eta_1 kT$, $\alpha_2 = q/\eta_2 kT$, $I_{o1}$ and $I_{o2}$ are the saturation currents for the first and second junction, respectively. Here, $\eta_1$ and $\eta_2$ are the ideality factors of the first and second junction, respectively. The room temperature $I$–$V$ characteristics of pristine and irradiated GaAs $p$–$i$–$n$ diode are shown in Fig. 1. The inset of Fig. 1 shows an enlarged view of the forward bias semi logarithmic $I$–$V$ characteristics. It is observed that the forward log ($I$) vs. $V$ curve shows single slope for ideal diode without series resistance ($R_s = 0$) and saturation current of $\sim 10^{-8}$ A. For generation dominated mechanism, the saturation current is given by $I_{0gr} = aqon_i/2\tau_0$, where device area ($a$) = $8 \times 10^{-8}$ m$^2$, intrinsic carrier density ($n_i$) in GaAs = $1.69 \times 10^6$ cm$^{-3}$, depletion width at zero bias ($\omega$) = 0.9 µm and the life time of carriers ($\tau_0$) = $1.08 \times 10^{-12}$ s. The depletion width is calculated from the formula

$$\omega \sqrt{\frac{2\varepsilon V_{bi}}{q} \left[ \frac{N_n + N_p}{N_n N_p} \right]}$$

where $\varepsilon$ is the dielectric constant of the material, $V_{bi}$ is the built-in voltage, $N_n$ and $N_p$ are the carrier densities at the junction. However, the forward log ($I$) vs. $V$ curve for GaAs $p$–$i$–$n$ diode shows two regions (with two different slopes) at low and high bias voltages, which indicates the presence of two diodes and a resistance ($R_s$) connected in series (as shown in the insets of Fig. 1). This is to be noted that the fitting of experimental $I$–$V$ curve of $p$–$i$–$n$ diode with transcendental Eq. (1) does not provide an explicit set of parameters. However, under such conditions, a curvature function is better sought which is referred as the beta function ($\beta$-model) proposed by Kavasoglu et al. [23,24]. According to $\beta$-model, the ideality factors of a $p$–$i$–$n$ device can be calculated from the curvature function ($\beta$), which is the ratio of the second derivative to the second power of the first derivative of the $I$–$V$ characteristic. Therefore, using Eq. (1), the curvature function $\beta$ becomes,

$$\beta = -\frac{(d^2V/dI^2)}{(dV/dI)^2} = \frac{(1/\alpha_1(I_{01}+I)^2 + 1/\alpha_2(I_{02}+I)^2)}{(1/\alpha_1(I_{01}+I) + 1/\alpha_2(I_{02}+I) + R_s)^2} \tag{2}$$

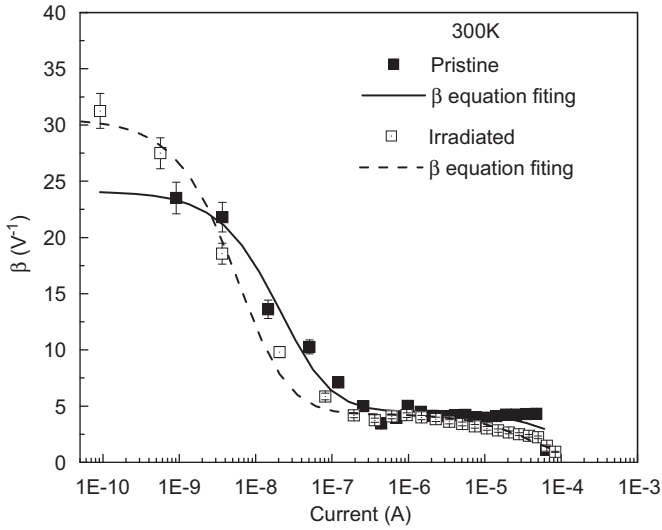**Fig. 2.** $\beta$-log $I$ characteristics of the pristine and irradiated $p$–$i$–$n$ diode at $T = 300$ K.

**Table 1**
Summary of GaAs $p$–$i$–$n$ diode parameters, (a) pristine, and (b) irradiated.

| Temperature (K) $\pm 0.2$ | $\eta_1 \pm 0.1$ | $I_{01}(A) \pm 2 \times 10^{-11}$ | $\eta_2 \pm 0.1$ | $I_{02}$ (A) $\pm 2 \times 10^{-11}$ | $R_s$ ($\Omega$) $\pm 50$ |
|---|---|---|---|---|---|
| (a) | | | | | |
| 125 | 2.2 | $1 \times 10^{-10}$ | 3.6 | $2.3 \times 10^{-8}$ | 1175 |
| 200 | 1.8 | $6 \times 10^{-10}$ | 4.9 | $3 \times 10^{-8}$ | 1048 |
| 300 | 1.5 | $1.2 \times 10^{-9}$ | 7.2 | $2 \times 10^{-7}$ | 858 |
| (b) | | | | | |
| 125 | 1.4 | $4 \times 10^{-11}$ | 6.5 | $9 \times 10^{-9}$ | 4531 |
| 200 | 1.3 | $8 \times 10^{-11}$ | 6.8 | $2 \times 10^{-8}$ | 3534 |
| 300 | 1.2 | $3 \times 10^{-10}$ | 8.0 | $8 \times 10^{-8}$ | 2789 |

By plotting $\beta$–$I$ curve, one can estimate the $\eta$'s for the two junctions, $R_s$ and the saturation currents by fitting the experimental data with Eq. (2). It is to be noted that the derivative at a point is computed by taking the average of the slopes between the point and its two nearest neighbors. It is written mathematically as $f'(x_i) = \frac{1}{2} \left( \frac{y_{i+1} - y_i}{x_{i+1} - x_i} + \frac{y_i - y_{i-1}}{x_i - x_{i-1}} \right)$. Here $y_i = f(x_i)$ and the second derivative is calculated by differentiating the first derivative. In our calculations, the difference between the two nearest points is 50 mV. Fig. 2 shows the room temperature $\beta$–$I$ curves for the pristine and irradiated $p$–$i$–$n$ devices along with the respective fitted curves. The values of $\eta_1$, $I_{o1}$, $\eta_2$, $I_{o2}$, $R_s$ are obtained by fitting the experimental data with Eq. (2). The obtained values of parameters for pristine and irradiated samples at room temperature are given in Table 1. Subsequently, the same exercise is carried out at other temperatures, where representative plots are shown only at 125 K and 200 K in Figs. 3 and 4 and the obtained parameters are listed in Table 1(a) and (b), respectively. The value of $R_s$ increases from 858 to 1175 $\Omega$ when the device temperature is reduced from 300 to 125 K. This is mainly due to the reduction of charge carrier density in the $i$-region. Furthermore, the values of $R_s$ in irradiated diodes are larger than those for the pristine diodes, irrespective of the temperature of measurements, confirming that the increase in resistance is due to the creation of defects. Further, as can be seen from Table 1(a) and (b), $\eta_1$ decreases from 2.2 to 1.5 and $\eta_2$ increases from 3.6 to 7.2 with heating from 125 to 300 K. The temperature dependent behaviors of $p$–$i$ and $i$–$n$ junctions are similar to the observations of T. L. Tansley et al. [30] and H. C. Torrey et al. [31] for separate $p$–$i$ and $i$–$n$ junctions. From these observations, one can represent the first
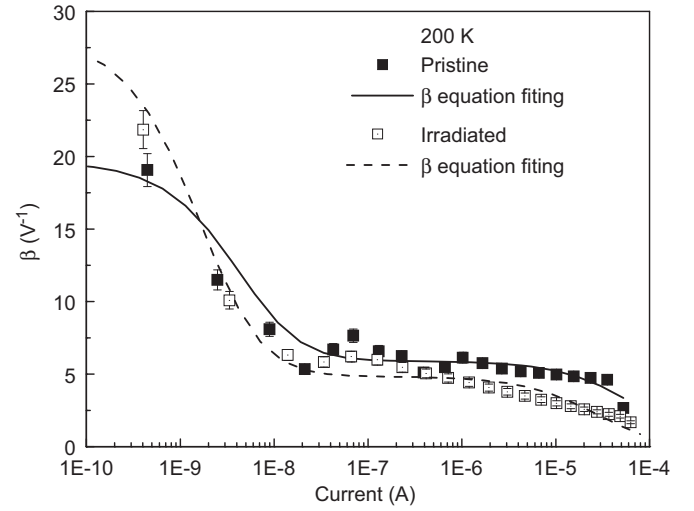


**Fig. 3.** $\beta$-log $I$ characteristics of the pristine and irradiated $p$–$i$–$n$ diode at $T = 200$ K.
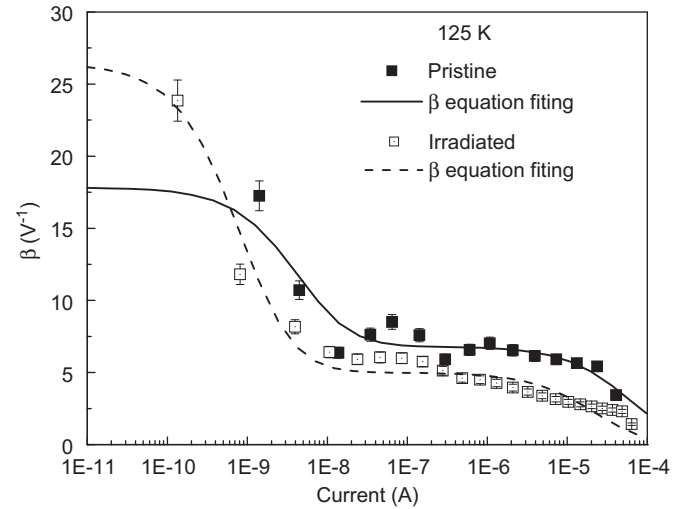


**Fig. 4.** $\beta$-log $I$ characteristics of the pristine and irradiated $p$–$i$–$n$ diode at $T = 125$ K.

junction as $p$–$i$ and the second junction as $i$–$n$ junction in the $p$–$i$–$n$ diode. It means that the $\eta_1$ & $I_{o1}$ are the ideality factor and saturation current of the $p$–$i$ junction, whereas $\eta_2$ and $I_{o2}$ are the ideality factor and saturation current of the $i$–$n$ junction. Further, after irradiation the ideality factor of the first junction decreases while that of the second junction increases. The increased ideality factor for the second junction is due to the enhanced recombination probability of carriers at the trap centers in the intrinsic region. Therefore, it is confirmed that after the irradiation the density of acceptor like trap centers increases substantially in the intrinsic region. The increased density of acceptor like states is also evident by the increased $R_s$, which are acting as the recombination centers in the $i$–$n$ junction.

Further, the saturation currents decrease after the $\gamma$-ray irradiation. This may be due to the reason that the charge carrier mobility is decreased after irradiation due to the scattering of carriers from the charged defects. In addition, the dark current also decreases under the reverse bias voltage (as shown in the inset of Fig. 1). The dark current is reduced predominantly due to decrease in the carrier mobility as well as increase in the compensation of the $i$-layer by removal of majority carriers from
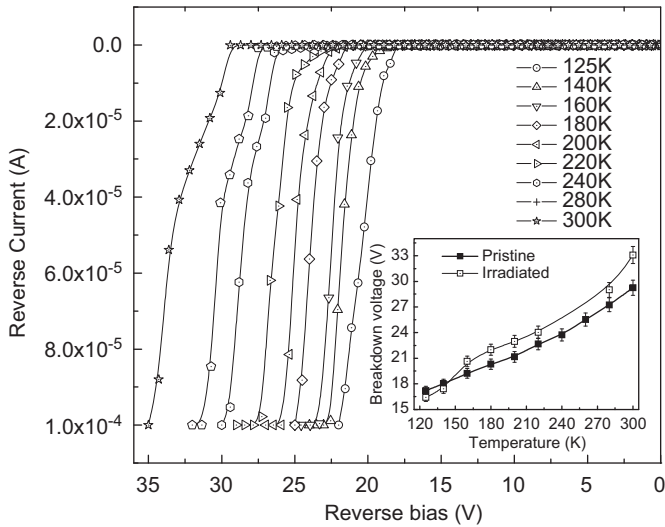
**Fig. 5.** Temperature dependent reverse *I–V* characteristics of the *p–i–n* diode. Inset shows the variation of reverse breakdown voltage with temperature.

it. Such a decrease of the dark current has been already observed for GaAs based materials including the quantum wells [32]. However, in some cases, the dark current increases after irradiation as reported in our previous article [21]. It is known from the literature that at low fluences the degradation is mainly due to the introduction of non-radiative recombination centers and for the large fluences, the compensation mechanism plays a significant role [33,34]. In our previous work, we have observed the compensation of majority carriers even at a moderate dose (Fig. 1(b) of Ref. [21]), but this may be less significant at lower doses and hence the dark current is increased. However, large radiation doses may lead to an increased compensation of the majority carriers which may significantly reduce the dark current. An increase of the series resistance from pristine to the γ-ray irradiated samples also indicates reduction of the majority carrier concentration and the mobility.

Fig. 5 shows the reverse bias *I–V* characteristics of the GaAs *p–i–n* diode in a temperature range of 125–300 K. It is observed that the value of the reverse breakdown voltage increases with heating. The variation of the breakdown voltage with temperature can be understood in terms of scattering of the charge carriers by phonons. The charge carriers passing through the depletion layer under a high electric field transfer a part of their kinetic energy to optical phonons after traveling a distance of the order of electron–phonon mean free path ($\lambda$). The value of $\lambda$ decreases with heating. Therefore, the carriers transfer more energy to the crystal lattice over a given distance at a constant electric field at higher temperatures. Hence, the carriers must pass through a greater potential difference before they can acquire sufficient energy to generate an electron–hole pair. Further, it should be noted that because of the compensation of charge carriers in the *i*-region, the band alignment of the *i*-layer with *p* and *n*-type layer changes, which in turn changes the built-in electric field. This also affects the breakdown voltage. However, the two mechanisms can be separated out by the sign of the observed temperature coefficient. The temperature coefficient of the avalanche breakdown voltage for *p–i–n* GaAs diode is given as $r=(\Delta V_B/V_B)(1/\Delta T)$, where, $V_B$ is the breakdown voltage at a given temperature, $\Delta V_B$ is the difference in breakdown voltage and $\Delta T$ is the temperature variation. Here, we observe a positive temperature coefficient, which confirms that the junction breakdown is predominantly due to the avalanche multiplication process [35–37].

Further, this is to be noted that the variation in breakdown voltage with temperature depends on the carrier density and impurity concentration in the *i*-layer that is used in the *p–i–n* diode. The theoretically predicted value of $r$ is $9 \times 10^{-4}$ ($K^{-1}$) and it can vary depending on the background impurity in the materials [38]. Hence, for the temperature measurement range of 125–300 K, the theoretically estimated value of $\Delta V_B$ varies from 6 to 10 V depending on the impurity concentration of the semiconductor materials. However, it is experimentally observed that the maximum breakdown voltage can be 10 V within the above temperature measurement range [39–40]. We also observe that the values of $\Delta V_B$ remain within the above range. Further, the values of reverse breakdown voltage increase after irradiation as shown in Fig. 1 and the inset of Fig. 5. At 300 K, the breakdown voltage increases from $30 \pm 0.5$ to $33 \pm 0.5$ V from pristine to the irradiated device. This may be due to the reduced mean free path of electrons because of the increased scattering from the radiation induced defects. Therefore, the carriers transfer more energy to the crystal lattice and to acquire sufficient energy for creating electron–hole pairs, the carriers must pass through greater potential difference. Hence, the value of $V_B$ increases after irradiation. The difference in breakdown voltage reduces with the cooling. It is noted that as the temperature is reduced to ~160 K, the breakdown voltage remains almost same for both the pristine and the irradiated devices which is due to the significant reduction of electron–phonon scattering at low temperatures. Therefore, the carriers transfer some energy in the crystal lattice and acquire similar energy for creating electron–hole pairs for pristine and the irradiated devices.

## Conclusion

GaAs *p–i–n* diodes were subjected to $^{60}$Co γ-ray irradiation and the effects of γ-ray irradiation on the *I–V* characteristics of the diodes have been studied using temperature dependent *I–V* measurements. The ideality factors, dark current and the series resistance for the two separate junctions *p–i* and *i–n* are extracted from the forward bias current–voltage measurements and using the β model. It is found that the series resistance increases with the γ-ray irradiation. The $R_s$ increases due to the enhanced recombination of carriers via trapping by the radiation induced defects. The defect density increases with irradiation because carbon impurities change their position from Gallium to Arsenic sites and subsequently transform them to acceptors like states and therefore increase the resistance of the diode. Further, the dark currents for the *p–i–n* diodes reduced after γ-ray irradiation. This is due to the reduction of electron mobility because of the additional scattering centers and enhanced compensation of majority carriers in the acceptor like trap states. Further, after irradiation, the ideality factor of the *p–i* junction decreases while that of the *i–n* junction increases. The increased ideality factor for the later junction is due to an enhanced recombination probability of carriers at the trap centers in the intrinsic region. Positive temperature coefficient of breakdown voltage confirms that the junction breakdown is due to the avalanche multiplication process. The variation of the breakdown voltage with temperature is dominated by the scattering of charge carriers by phonons. The charge carriers passing through the depletion layer under a high electric field transfer a part of their kinetic energy to phonons after traveling one electron–phonon mean free path. The value of mean free path decreases with heating. Therefore, the carriers lose more energy to the crystal lattice and thus require greater potential difference for acquiring sufficient energy to generate an electron–hole pair. Further, the breakdown voltage increases after irradiation due to increased scattering from the

generated defects which leads to the reduction of the mean free path of electrons and hence requires a large potential to generate the electron–hole pairs.

## Acknowledgments

## References

[1] T. Lai, D. Alexiev, B.D. Nener, Journal of Applied Physics 78 (1995) 3686.
[2] M. Edwards, G. Hall, S. Sotthibandhu, Nuclear Instruments and Methods A 310 (1991) 283.
[3] S. Tataroğlu, M.M.Bülbül Altındal, Nuclear Instruments and Methods A 568 (2006) 863.
[4] V.A.J. Vanlint, Nuclear Instruments and Methods A 253 (1987) 453.
[5] G.E. Brehm, G.L. Pearson, Journal of Applied Physics 43 (1972) 568.
[6] H.W. Kunert, D.J. Brink, Journal of Applied Physics 81 (1997) 6948..
[7] C. Bjorkas, K. Nordlund, K. Arstila, J. Keinonen, V.D.S. Dhaka, M. Pessa, Journal of Applied Physics 100 (2006) 053516.
[8] Anna Cavallini, Laura Polenta, Journal of Applied Physics 98 (2005) 023708..
[9] J.G. Williams, J.U. Patel, A.M. Ougouag, S.Y. Yang, Journal of Applied Physics 70 (1991) 4931.
[10] J.U. Patel, J.G. Williams, G.E. Stillman, Journal of Applied Physics 73 (1993) 3734.
[11] M.J. Romero, D. Araujo, R. Garcia, R.J. Walters, G.P. Summers, S.R. Messenger, Applied Physics Letters 74 (1999) 2684.
[12] J.C. Pigg, J.H. Crawford, Journal of Physical Review 135 (1964) A1141.
[13] J. Wang, W. Yang, Nuclear Instruments and Methods B 266 (2008) 3583.
[14] M. McPherson, B.K. Jones, T. Solan, Semiconductor Science and Technology 12 (1997) 1187.
[15] M. McPherson, Journal of Optics A: Pure and Applied Optics 7 (2005) 325.
[16] K.M. Smith, Nuclear Instruments and Methods A 368 (1995) 220.
[17] B.K. Jones, J. Santana, M. McPherson, Nuclear Instruments and Methods A 395 (1997) 81.
[18] G.F. Knoll, Radiation Detection and Measurement, John Wiley & Sons, Inc., 1979.
[19] S. Karatas, A. Turut, S. Altındal, Nuclear Instruments and Methods A 555 (2005) 260.
[20] T. Hashizume, H. Hasegawa, Journal of Applied Physics 68 (1990) 4598.
[21] S.K. Khamari, V.K. Dixit, T. Ganguli, S. Porwal, S.D. Singh, S. Kher, R.K. Sharma, S.M. Oak, Nuclear Instruments and Methods B 269 (2011) 272.
[22] D.C. Look, Electrical Characterization of GaAs Materials and Devices, John Wiley & Sons, Singapore, 1989.
[23] N. Kavasoglu, A.S. Kavasoglu, S. Oktik, Current Applied Physics 9 (2009) 833.
[24] A.S. Kavasoglu, N. Kavasoglu, Current Applied Physics 9 (2009) 894.
[25] V.K. Dixit, T.K. Sharma, T. Ganguli, S.D. Singh, S. Porwal, R. Kumar, Proceedings of the 50th DAE, S.S.P.S. December 2005, BARC, Mumbai.
[26] S.K. Khamari, V.K. Dixit, T. Ganguli, S. Porwal, S.D. Singh, S. Kher, R.K. Sharma, S.M. Oak, Proceedings of the N.S.N.I., 259, 2010, BARC, Mumbai, India.
[27] S. Kher, P. Joshi, R.K. Sharma, Nuclear Instruments and Methods A 578 (2007) 345.
[28] P.K. Kush, R.C. Sharma, R.S. Doohan, A.K. Sagar, C.L. Choudhary, M.S. Ansari, Proceedings of National Seminar and Conference on Cryogenics and its Frontier applications, 25–27 March 2004, Howrah, India, p. 12.
[29] D.K. Schroder, Semiconductor Material and Device Characterization, John Wiley & Sons, 1990.
[30] T.L. Tansley, S.J.T. Owen, Journal of Applied physics 55 (1984) 454.
[31] H.C. Torrey, C.A. Whitmer, Crystal Rectifiers, McGraw Hill, New York, 1948, Chapter 8.
[32] V. Doncheva, J.C. Bourgoina, P. Bois, Nuclear Instruments and Methods A 517 (2004) 94.
[33] A. Rao, S. Krishnan, G. Sajeev, K. Siddappa, Pramana-Journal of Physics 74 (2010) 995.
[34] J.C. Bourgoin, M. Zazoui, Semiconductot Science and Technology 17 (2002) 453.
[35] W.I. Khan, Solid-State Electronics 31 (1988) 1265.
[36] R.L. Aggarwal, I. Melngailis, S. Verghese, R.J. Molnar, M.W. Geis, L.J. Mahoney, Solid-State Communications 117 (2001) 549.
[37] C.R. Crowell, S.M. Sze, Applied Physics Letters 9 (1966) 242.
[38] S.M. Sze, Physics of Semiconductor Devices, John Wiley & Sons, Singapore, 2005.
[39] Y.K. Su, S.Y. Chang, T.S. Wu, Optical and Quantum Electronics 11 (1979) 109.
[40] R. Singh, S.K. Arora, R. Tyagi, S.K. Agarwal, D. Kanjilal, Bulletin of Materials Science 23 (2000) 471.